A Low-Power OAM Metasurface for Rank-Deficient Wireless Environments

Kun Woo Cho, Srikar Kasi, Kyle Jamieson

Princeton University

***Abstract*—This paper presents Monolith, a high bitrate, low-power, metamaterials surface-based Orbital Angular Momentum (OAM) MIMO multiplexing design for rank deficient, free space wireless environments. Leveraging ambient signals as the source of power, Monolith backscatters these ambient signals by modulating them into several orthogonal beams, where each beam carries a unique OAM. We provide insights along the design aspects of a low-power and programmable metamaterials-based surface. Our results show that Monolith achieves an order of magnitude higher channel capacity than traditional spatial MIMO backscattering networks.**

***Index Terms*—Orbital angular momentum, metasurface, cellular wireless networks**

I. Introduction

The multiple-input multiple-output (MIMO) system enables a plethora of applications that require high traffic volume, such as 5G services in urban canyons and indoor VR/AR, by establishing independent parallel channels between multiple transmit and receive antennas. However, the capacity offered by spatial MIMO systems largely relies on multi-path components, and so the practical applicability of such systems is challenging in many *rank-deficient* application scenarios such as farm fields in smart agriculture and satellite channels in space communication. Further issues surrounding the power consumption of such MIMO systems, including that of power-hungry radio frequency (RF) chains whose power requirements scale proportionally with the number of antennas, constrain the applicability of spatial MIMO systems even further. Today's emerging wireless applications in rank-deficient environments (*e.g.,* agriculture and weather monitoring in smart farm [1] and mega-constellation satellites [2]) also demand high bandwidth, implying that power availability at edge devices is becoming a more critical issue which ultimately will restrict such applications from adopting spatial MIMO systems.

To address these issues, we introduce **Monolith**, a reconfigurable metamaterial surface that backscatters the signal into several multiplexed orthogonal beams. Each of the multiplexed beams carry a "unique" orbital angular momentum (OAM) state which enables orthogonality for beams with different OAM states. OAM state can be equivalently thought of as the number of phase rotations applied to the incoming signal, and so a beam with non-zero OAM state takes on a helical shape in the direction of propagation. Since Monolith itself generates multiple orthogonal beams, it eliminates the need of rich scattering environments for spatial multiplexing.

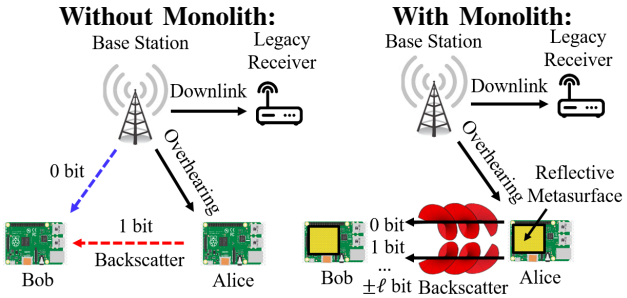

(a) Ambient backscatter system for edge devices.

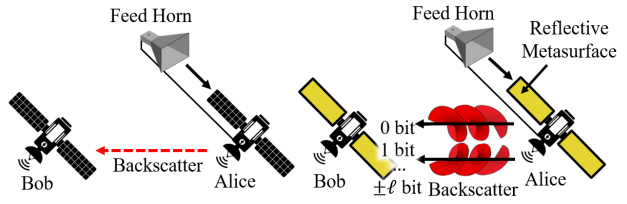

(b) Reflectarray antenna for satellite communication.

Fig. 1: Various use cases for Monolith. The sender (Alice) backscatters the signals, and the reader (Bob) decodes the signals. With Monolith, a metasurface artificially creates multiple orthogonal beams and spatially multiplexes them.

We believe Monolith will expand the applicability of MIMO in the following rank-deficient application scenarios:

1. Ambient backscattering for low-power devices. Ambient backscattering [3], [4] offers ultra-low energy consumption by enabling sensory devices to pick up an ambient signal, harvest it as the source of power, and then reflect it with encoded data, such that these devices can communicate without generating and transmitting their own signals. Eliminating the need for active transmitter and power-consuming RF components significantly lowers the energy burden and therefore enables edge devices in rural and remote areas to operate on a smaller battery or even a batteryless device. While state-of-the-art ambient backscattering systems are extremely low bit-rate, Monolith enhances the link capacity of ambient backscattering systems by adopting OAM spatial multiplexing. In conventional ambient backscatter networks (Fig. 1(a) on left), the sender indicates either a '0' or a '1' bit by switching its antenna between reflecting and non-reflecting states. In Monolith (Fig. 1(a) on right), on the other hand, the sender converts

the ambient signal into several multiplexed orthogonal beams wherein each beam supports a different data bit. The receiver later separates the multiplexed beams.

2. Reflectarray antenna system for satellites. To achieve a high gain, low profile, and light-weight communication system, satellites deploy a reflectarray antenna that consists of a feed horn and a planar structure of reflecting elements [5], [6], [7]. Specifically, the horn excites the array, which in turn steers the reflected beam according to its configuration. To maximize the link capacity of satellites, Monolith utilizes an OAM metasurface as the reflecting antenna array. As shown in Fig. 1(b), the surface transforms the signals from the horn into multiple orthogonal beams and spatial multiplexes them on the space. We note that the use of extremely high frequency in satellite communication [8] mitigates the divergence of OAM beams, rendering OAM-MIMO to be more practical and deployable. We will further discuss the beam divergence in §IV.

In this paper, we present an in-depth analysis on OAM multiplexing and demonstrate that OAM-based MIMO systems achieve significantly higher wireless capacity than the traditional MIMO system in rank-deficient wireless environments. Our further studies elaborate on Monolith's system architecture, ranging from its surface design to its encoding and decoding schemes, along with simulated results that project the feasibility of Monolith.

II. Primer: Orbital Angular Momentum

From Maxwell's theory, it is known that electromagnetic (EM) waves carry both linear momentum and angular momentum. The angular momentum has two independent attributes: a spin angular momentum (SAM) associated with the polarization of the EM wave, and an orbital angular momentum (OAM) associated with the spatial distribution of the EM wave fields [9]. In particular, OAM beams carry a twisted/helical phase front that rotates as the beam propagates. This helical phase can be manipulated by generating phase twists across multiple transmitting antennas. Let us define the number of phase twists as a *state*. By increasing the number of phase twists, OAM can theoretically have "infinite" states, each corresponding to a distinct topological charge [10]. Moreover, OAM beams with different states are mutually orthogonal in spatial domain, thus offering a possibility of unlimited, parallel channels for data transmission. Figure 2 illustrates an example metasurface that reflects and converts a Gaussian beam with no OAM into multiplexed OAM beams with five different OAM states (l = +2, +1, 0, −1, or −2) along with the phase and intensity profile of each OAM beam. The intensity nulls at the center, and it expands as the absolute value of OAM state increases.

In this section, we address a recent controversy over OAM and investigate the advantages of OAM-based multiplexing over the conventional MIMO multiplexing.

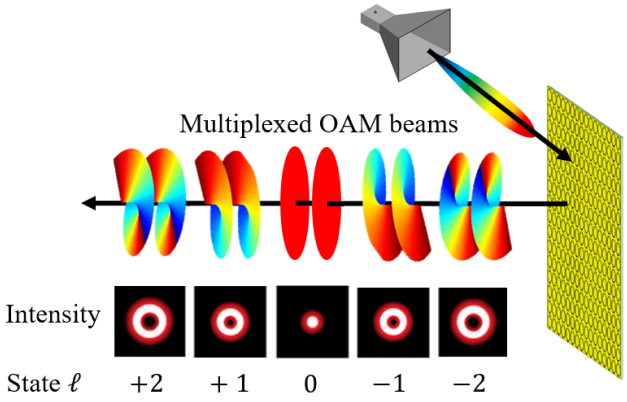

Fig. 2: Mixed-state OAM generation using Monolith.

A. Is OAM a new concept?

After Tamburini *et al.* [11] argued that the OAM is a new degree of freedom that allows an unlimited use of wireless channels on the same frequency, there was controversy over whether OAM enables a new and distinct physical degree of freedom [11], [12] or is simply a subset of MIMO [13], [14]. OAM beams with different states are intrinsically orthogonal to each other, providing a new opportunity to spatially multiplex different beams along the same physical paths. Since MIMO is a general technique dealing with the use of multiple antennas and multipath propagation, OAM is in fact a special form of MIMO [14] and does not provide a new degree of freedom. Unlike traditional MIMO, OAM does not need a large number of unrelated paths for spatial reuse (and indeed, cannot leverage physical paths reflecting off objects in the environment) because different OAM beams themselves are orthogonal. Therefore, OAM-MIMO communication fills the need for spatial multiplexing in the absence of a rich scattering environment, while conventional MIMO retains its utility in the presence of a rich scattering environment.

Earlier studies [14] on OAM generation utilize a uniform circular array (UCA) where each adjacent array element adopts excitation feed with equal amplitude and $2\pi l/N$ phase difference. However, a UCA requires a large number of antennas to generate high-order OAM state and has a large beam divergence angle. Also, it requires power-hungry phase shifters, which is not suitable for low-power devices. Very recently, artificially-engineered surfaces, called *meta-surfaces*, have been studied to manipulate the EM wave properties [15], [16]. Compared to UCAs, metasurfaces have advantages of low power, high gain, and flexible capability of modulating EM waves. Recently, Ref.[17] proposed a 1-bit reconfigurable metasurface to generate different OAM beams by loading the PIN diode (*i.e.* on-off switch) on each element of metasurface. Similarly, [18], [19] demonstrated state-reconfigurable OAM metasurfaces using varactor diodes for finer phase control. In this paper, we explore varactor-loaded metasurfaces for a better control of OAM phase profiles.

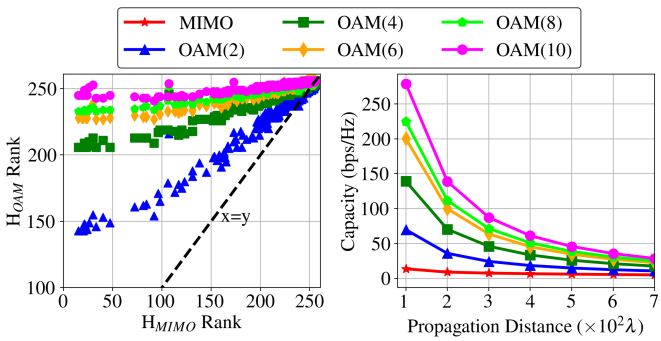

Fig. 3: *Left:* Channel rank enhancement by OAM. *Right:* Capacity comparison between OAM and MIMO.

B. Understanding the benefits of OAM

In this section, we explain metasurface-based OAM multiplexing's capacity gains using standard MIMO theory. We demonstrate that OAM-based MIMO communication achieves a significant capacity gain over traditional MIMO communication when the rank of channel is low.

Channel Model. In free-space MIMO systems, the channel matrix is expressed as $\mathbf{H}_{\text{MIMO}} = [h_{mn}^{\text{MIMO}}]_{M\times N}$, where h_{mn}^{MIMO} is channel response between n^{th} transmitting antenna and m^{th} receiving antenna. It takes the form:

$$h_{mn}^{\text{MIMO}} = \beta \frac{\lambda}{4\pi d_{mn}} e^{-j\frac{2\pi}{\lambda}d_{mn}} \tag{1}$$

where β is a constant containing attenuation and phase associated with the antenna system configuration, λ is the carrier wavelength, and d_{mn} is the distance the signal propagates. Similarly, in OAM-based MIMO systems, the channel matrix is expressed as $\mathbf{H}_{\text{OAM}} = [h_{mn}^{\text{OAM}}]_{M\times N}$, where h_{mn}^{OAM} can be modeled as MIMO channel response superimposed by a spiral phase factor. It takes the form:

$$h_{mn}^{\text{OAM}} = h_{mn}^{\text{MIMO}} \cdot e^{j\widetilde{l}_n \widetilde{\varphi}_{mn,l}} \tag{2}$$

where $\widetilde{l}_n$ contains all Q number of OAM states generated by the n^{th} transmit antenna, and $\widetilde{\varphi}_{mn,l}$ denotes the cumulative phase of the l-labeled OAM state after propagation from n^{th} transmit to m^{th} receive antenna.

Our Scenario. In our system, the transmitting and receiving elements are *meta-atoms*, and they are arranged in a uniform rectangular array pattern on a substrate we refer to as a *metasurface* (details are provided in Sec. III, Fig. 4 depicts this scenario for a 16×16 metasurface system). Let us assume that both the transmitting and receiving metasurfaces consist equal number of meta-atoms. Then, the propagation distance ($d_{(p,q),(s,t)}$) between the $(s,t)^{th}$ transmit and $(p,q)^{th}$ receive meta-atoms is:

$$d_{(p,q),(s,t)} = \sqrt{D^2 + \Delta^2\{(p-s)^2 + (q-t)^2\}} \tag{3}$$

where D is the distance between the center of transmitting and receiving metasurfaces, and Δ is the spacing between consecutive meta-atoms. (p,q) and (s,t) indicate the (row, column) locations of the receive and transmit meta-atoms in their respective metasurfaces. The cumulative OAM phase factor corresponding to these meta-atoms is then:

$$\widetilde{\varphi}_{(p,q),(s,t),l} = \phi_{(p,q),(s,t)} + \frac{2\pi}{\lambda}\tilde{l}_{(s,t)}D \tag{4}$$

where $\phi_{(p,q),(s,t)}$ is the azimuthal angle between the $(s,t)^{th}$ transmit meta-atom and $(p,q)^{th}$ receive meta-atom along the axis of propagation, which depends only on the relative locations of these meta-atoms. It can be calculated as [20]:

$$\phi_{(p,q),(s,t)} = \begin{cases} tan^{-1}(|p-s|/|q-t|), & p>s, q>t \\ \pi - tan^{-1}(|p-s|/|q-t|), & p>s, q<t \\ \pi + tan^{-1}(|p-s|/|q-t|), & p<s, q<t \\ 2\pi - tan^{-1}(|p-s|/|q-t|), & p<s, q>t \\ 0, & p=s, q\geq t \\ \pi/2, & p>s, q=t \\ \pi, & p=s, q<t \\ 3\pi/2, & p<s, q=t \end{cases} \tag{5}$$

Using Eqs. 1 and 3, we obtain $\mathbf{H}_{\text{MIMO}}$, and using Eqs. 1–5, we obtain $\mathbf{H}_{\text{OAM}}$. We next demonstrate benefits of OAM.

Simulation Results. In MIMO communication systems, the rank of the channel matrix is an indicator for the number of data streams that can be spatially multiplexed on the channel. Therefore, higher rank channels provide more wireless capacity. To understand the impact of OAM on MIMO channel rank, we first investigate in Fig. 3 (*left*) how the rank of $\mathbf{H}_{\text{OAM}}$ compares with that of $\mathbf{H}_{\text{MIMO}}$. For this evaluation, we consider an $M = N = 256$ metasurface system. The carrier frequency and corresponding wavelength (λ) are set to 2.4 GHz and 124.91 mm respectively, the meta-atom spacing Δ is 20 mm, and the gain coefficient β is 40 dB. The distance D between transmit and receive metasurfaces is varied from $10^2\lambda$ to $10^5\lambda$ in steps of $10^2\lambda$, where each step results in a different channel matrix. OAM(Q) indicates Q different OAM states are generated by transmit meta-atoms (*i.e.,* $\widetilde{l}_n = n\%Q$). The figure shows that OAM-based MIMO systems achieve higher channel rank than traditional MIMO system under similar channel conditions, and that the $\mathbf{H}_{\text{OAM}}$ rank increases with increasing the number of OAM states. This rank enhancement is a result of the additional spiral phase factor (Eq. 2) conditioned in OAM-based MIMO systems.

We next compare in Fig. 3 (*right*) the end-to-end channel capacity performance of OAM-based MIMO systems against the traditional MIMO system. The capacity is computed as:

$$C = \sum_{i}^{\gamma} \log_2\left(1 + \frac{P_i}{\sigma^2/\delta_i^2}\right) \text{ bps/Hz} \tag{6}$$

where γ is the channel matrix rank, σ^2 is the channel noise variance, and δ_i is the i^{th} singular value obtained via singular value decomposition of the channel matrix. The total transmit power budget is set to one Watt, allocated proportionally to

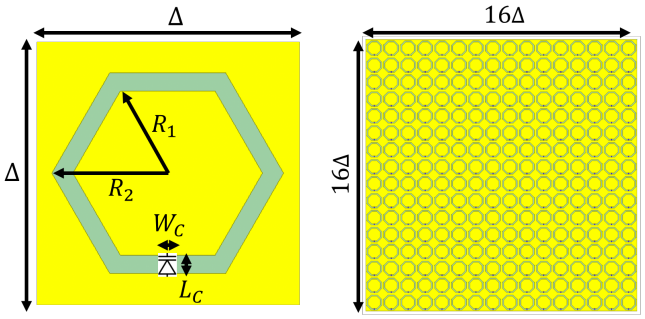

(a) Meta-atom design. **(b)** Monolith design.

Fig. 4: Schematic model of meta-atom and metasurface. Our meta-atom consists of several design parameters, including Δ, R_1, R_2, W_c, and L_c.

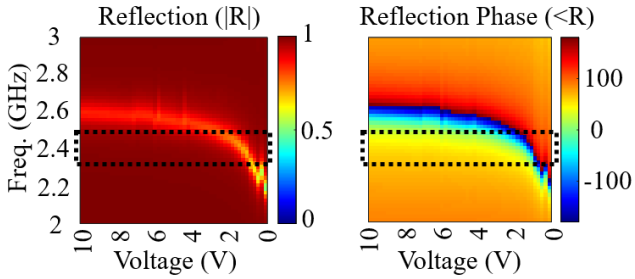

Fig. 5: *Left:* simulated magnitude; *right:* phase of reflected coefficient for the meta-atom across different voltage values from 0 to 10 V.

all transmit meta-atoms (P_i). The figure shows that OAM-based MIMO systems achieve significantly higher wireless capacity than the traditional MIMO system. At a propagation distance of 200λ, traditional MIMO achieves a capacity of 8.98 bps/Hz, whereas OAM-MIMO with 2, 4, 6, 8, and 10 states achieves 35.90, 70.43, 99.86, 111.71, and 138.91 bps/Hz capacity performance respectively.

III. Monolith Design

We now introduce Monolith, a metamaterials-based programmable surface design that transforms an incident Gaussian beam into multiple OAM orthogonal beams with different topological charges. We will describe our surface design as well as its encoding and decoding scheme.

A. Surface Design

Figure 4 shows Monolith design architecture, consisting of its core building blocks, *meta-atoms*. Each meta-atom is an independently controllable scatterer that locally alters the phase of the incident wave. Here we first describe our meta-atom design and then present how we leverage Monolith to generate multiple OAM beams.

Meta-atom. Figure 4(a) shows our meta-atom (hexagonal structure), made up of copper material that lays on top of a dielectric substrate (green/light shade layout). A varactor diode (*i.e.,* a voltage-dependent capacitor) connects the inner and outer metal patches of the meta-atom. By controlling voltage levels across the varactor diode, we can change its capacitance and in turn alter the meta-atom's response to incident wave's EM field. To understand this phenomenon more clearly, let us model the load impedance across the meta-atom as $Z_{eff} = jwL + \frac{1}{jwC}$, where L and C are the inductance and capacitance of the meta-atom, respectively. By applying a certain voltage value across the varactor, we alter C and obtain a new load impedance Z_{eff}^{new}. This new load impedance then results in a new electromagentic response to the incident wave. Figure 5 illustrates the magnitude (*Left*) and phase (*Right*) response of EM waves reflected from the meta-atom as we apply different voltage values. By applying voltage from 0 to 10V, our meta-atom can provide up to 2π phase shift with a near-perfect reflection magnitude within 2–3 GHz. Using this technique, we will arbitrarily configure each meta-atom with a desired phase shift and form an OAM phase distribution across the entire metasurface.

Generating OAM Beams. Now, we will describe how we leverage the ensemble of many meta-atoms to generate OAM beams. A single metasurface layer is made up of 256 meta-atoms arranged in a 16×16 uniform rectangular array fashion as shown in Fig. 4(b). To generate each OAM beam as represented in Eq. 2, we configure the helical phase distribution ($e^{jl\varphi}$ term) by applying an appropriate voltage distribution across the surface. Specifically, we calculate a required phase shift per meta-atom for an OAM state l as:

$$\varphi(x, y) = l \cdot \tan^{-1}(y/x) - 2\pi/\lambda \cdot r_{xy} \tag{7}$$

where (x, y) indicates the coordinate location of each meta-atom in the surface plane with its center as an origin. λ is a carrier wavelength, and r_{xy} is the distance between the center of a transmitter and the coordinate (x, y), which is equivalent to $\sqrt{x^2 + y^2 + d^2}$. Here, d is the distance between an incident wave and the center of the metasurface. After acquiring the required phase distribution from Eq. 7, we use a genetic optimization algorithm to find a corresponding voltage distribution:

$$\Theta^* = argmin \sum_{x,y} (|F(V(x, y)) - \varphi(x, y)|) \tag{8}$$

where $F(V(x, y))$ represents the voltage-to-phase mapping function based on Fig. 5. Applying the foregoing OAM beam generation analysis, we present the phase and voltage distributions for each OAM beam with its topological charge $l = 0, 1,$ or 2 in Fig. 6. Since each surface layer is dedicated for a single OAM state, we stack several layers of the surface to multiplex different beams. We will explore an optimal stacking configuration in our future work.

Simulation Results. To evaluate Monolith's ability to generate different OAM states, we present our HFSS simulation results on Monolith. Figure 7 shows that Monolith can support

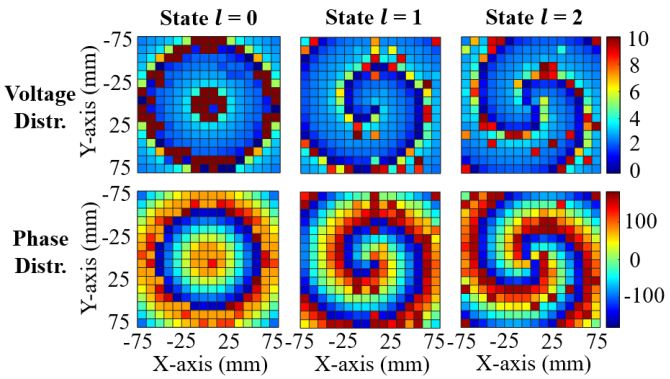

Fig. 6: *Upper:* an applied voltage distribution; *lower:* phase distribution by applying the voltage distribution. X- and Y-axis represent the coordinate of each meta-atom with the meta-atom at the center being (0,0) mm.

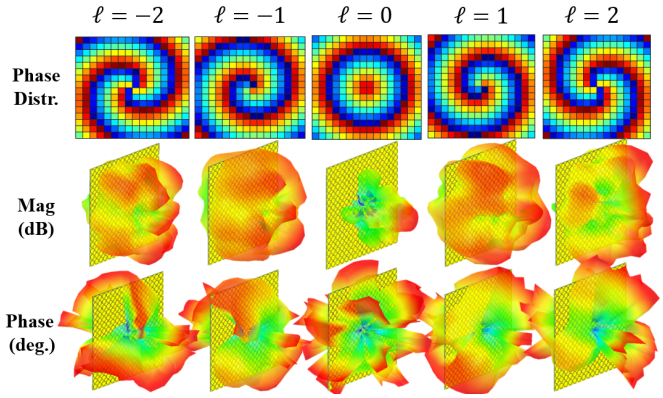

Fig. 7: *Upper:* a phase distribution of an OAM state from −2 to 2; *middle:* a magnitude of the generated OAM beams; *lower:* a phase of the generated OAM beams.

an OAM state l of −2, −1, 0, 1, and 2. We also observe that the beam with state $l = 0$ shows a high intensity at the center while the magnitude of the beams with non-zero OAM state nulls at the center. This nullified area expands as $|l|$ increases. Furthermore, Monolith creates one phase twist for OAM state +1/−1 and two phase shifts for OAM state +2/−2. Every beam with a positive-valued state complements its respective negative-valued state. These results thus comply with our theory, and we verify orthogonality of OAM beams with different states (§II).

B. Data Encoding and Decoding

In this section, we describe Monolith's data encoding and decoding schemes.

Encoding. In traditional ambient backscatter networks, the received signal at the reader can be expressed as:

$$y(t) = x(t) + \alpha b x(t) + w(t) \tag{9}$$

where $x(t)$ is an ambient signal from a base station, $w(t)$ is noise, α is an attenuation factor of backscattered signals relative to ambient signals, and b is a binary bit transmitted by the backscattering transmitter [3]. Similarly, we can represent the received signal of our OAM-based system as:

$$y(t) = x(t) * h_{env,r}(t) + (x(t) * h_{env,t}(t)) * h_{oam}(t) \cdot B + w(t) \tag{10}$$

where $h_{env,r}(t)$ and $h_{env,t}(t)$ are wireless channels between the base station and the reader and between the base station and the tag, respectively. Here, $*$ operator indicates convolution. $h_{oam}(t)$ is a multi-state OAM channel defined in Eq. 2, and B is a vector of the phase modulation $e^{j\theta_{l_1}(t)}$, $e^{j\theta_{l_2}(t)}$, ..., $e^{j\theta_{l_Q}(t)}$. Each phase modulation $e^{j\theta_{l_n}(t)}$ corresponds to an OAM state l_n, and Monolith manipulates the phase $\theta(t)$ according to the data that is being modulated. We note that OAM state of 0 (*i.e.* a Gaussian beam without OAM) is not multiplexed and thus it is not part of H_{OAM}.

Decoding. For traditional ambient backscatter networks, the receiver distinguishes reflected and non-reflected states using two power levels, $|1 + \alpha|^2 P$ and P. By doing so, they decode the information from backscattered signals [3]. Monolith, however, separates the signal in two stages. First, we separate h_{env} from received signals to extract h_{OAM}. Since h_{env} is a Gaussian beam without OAM, we can demultiplex it by applying a simple spatial filter. Then, for a mixed-state channel h_{OAM}, we transform each OAM beam back to a Gaussian beam using a mode-conversion spatial filter and successively cancel out from the mixed-state OAM channel until we decode all beams.

IV. Challenges and Discussion

Beam Divergence. OAM beams with higher-order states provide more capacity gains, but such beams physically diverge quickly, making it difficult for a receiver to fully capture OAM-multiplexed beams. To minimize the divergence of OAM, we must optimize many factors, including the carrier frequency, propagation distance, beam waist at the transmitter, and OAM state indices, Otherwise, the required receiver size becomes too large, rendering the OAM-MIMO system impractical. An alternative solution is to design a demultiplexing algorithm that captures and decodes only the partial area of the received beam where the orthogonality of different OAM states is preserved. This is feasible because the phase pattern repeats over different topological areas, and this repetition tends to occur more frequently when the state indices are low as shown in Fig. 6. By doing so, we can minimize the receiver size—we leave this for future work.

Beam Distortion. Since scatterers deteriorate the orthogonality of OAM beams, it is challenging to realize OAM-MIMO through such environments. We can mitigate the noise by using multi-plane-light converters (MPLCs) as a spatial filter. Specifically, MPLC shapes the EM wave at multiple propagating distances to accomplish mode conversion between OAM and Gaussian beams at different locations [10]. By doing so,

the patterns are updated using the wavefront matching method, which partially undo the effects of scattering.

Beam Steering. In line-of-sight (LoS) communication, alignment between the transmitter and receiver is crucial for sufficient signal power. Such alignment is even more important for OAM multiplexing systems because misalignment may cause crosstalk among channels. To mitigate misalignment, [21], [22] have explored the simultaneous generation and tunable steering of multiplexed OAM beams. Specifically, [19], [22] steer OAM beams by applying a proper phase distribution over different meta-atoms.

Backscatter Communication. Prior works on backscatter communication have mainly focused on sensor applications that require less than one Mbps. In particular, ambient backscatter communication [3], [4] was introduced to enable low-power, low data-rate device-to-device communication by backscattering ambient signals. While [23] has explored a way to increase the transmission range of such signals, our work in contrast focuses on increasing the link capacity of ambient backscattering via low-power OAM multiplexing techniques.

Optical Communications. Since the path between two satellites is free-space, inter-satellite networks commonly deploy free-space optical communication (FSO), which uses optical links to exchange data [8]. Specifically, [5], [6], [7] have used reflectarray antennas, which are placed on the satellite and excited via the feed horn. The use of extremely high frequency mitigates the beam divergence, rendering OAM-MIMO to be easily deployable without a complex receiver design.

V. Conclusion

This paper proposes a holistic OAM-based ambient backscatter design for rank-deficient wireless environments. We theoretically analyze the OAM-MIMO multiplexing and provide a preliminary study on generating the OAM beam with different states.

Acknowledgements

This material is based upon work supported by the National Science Foundation under Grant No. CNS-2148271 and is supported in part by funds from federal agency and industry partners as specified in the Resilient & Intelligent NextG Systems (RINGS) program. We gratefully acknowledge the support of a grant from the Princeton University School of Engineering and Applied Science Innovation Fund.

References

[1] R. Chandra and S. Collis, "Digital agriculture for small-scale producers: challenges and opportunities," *Communications of the ACM*, vol. 64, no. 12, pp. 75–84, 2021.

[2] M. Handley, "Delay is not an option: Low latency routing in space," in *Proceedings of the 17th ACM Workshop on Hot Topics in Networks*, HotNets '18, (New York, NY, USA), p. 85–91, Association for Computing Machinery, 2018.

[3] V. Liu, A. Parks, V. Talla, S. Gollakota, D. Wetherall, and J. R. Smith, "Ambient backscatter: Wireless communication out of thin air," *ACM SIGCOMM Computer Communication Review*, vol. 43, no. 4, pp. 39–50, 2013.

[4] S.-N. Daskalakis, J. Kimionis, A. Collado, M. M. Tentzeris, and A. Georgiadis, "Ambient fm backscattering for smart agricultural monitoring," in *2017 IEEE MTT-S International Microwave Symposium (IMS)*, pp. 1339–1341, IEEE, 2017.

[5] J. A. Encinar, M. Arrebola, F. Luis, and G. Toso, "A transmit-receive reflectarray antenna for direct broadcast satellite applications," *IEEE Transactions on Antennas and Propagation*, vol. 59, no. 9, pp. 3255–3264, 2011.

[6] D. R. Prado, A. Campa, M. Arrebola, M. R. Pino, J. A. Encinar, and F. Las-Heras, "Design, manufacture, and measurement of a low-cost reflectarray for global earth coverage," *IEEE antennas and wireless propagation Letters*, vol. 15, pp. 1418–1421, 2015.

[7] D. Martinez-de Rioja, E. Martinez-de Rioja, Y. Rodriguez-Vaqueiro, J. A. Encinar, and A. Pino, "Multibeam reflectarrays in ka-band for efficient antenna farms onboard broadband communication satellites," *Sensors*, vol. 21, no. 1, p. 207, 2020.

[8] M. A. Khalighi and M. Uysal, "Survey on free space optical communication: A communication theory perspective," *IEEE Communications Surveys*, vol. 16, no. 4, pp. 2231–2258, 2014.

[9] A. M. Yao and M. J. Padgett, "Orbital angular momentum: origins, behavior and applications," *Advances in optics and photonics*, vol. 3, no. 2, pp. 161–204, 2011.

[10] A. E. Willner, Z. Zhao, C. Liu, R. Zhang, H. Song, K. Pang, K. Manukyan, H. Song, X. Su, G. Xie, *et al.*, "Perspectives on advances in high-capacity, free-space communications using multiplexing of orbital-angular-momentum beams," *APL Photonics*, vol. 6, no. 3, p. 030901, 2021.

[11] F. Tamburini, E. Mari, B. Thidé, C. Barbieri, and F. Romanato, "Experimental verification of photon angular momentum and vorticity with radio techniques," *Applied Physics Letters*, vol. 99, no. 20, p. 204102, 2011.

[12] F. Tamburini, E. Mari, A. Sponselli, B. Thidé, A. Bianchini, and F. Romanato, "Encoding many channels on the same frequency through radio vorticity: first experimental test," *New Journal of Physics*, vol. 14, no. 3, p. 033001, 2012.

[13] M. Tamagnone, C. Craeye, and J. Perruisseau-Carrier, "Comment on 'encoding many channels on the same frequency through radio vorticity: first experimental test'," *New Journal of Physics*, vol. 14, no. 11, p. 118001, 2012.

[14] O. Edfors and A. J. Johansson, "Is orbital angular momentum (oam) based radio communication an unexploited area?," *IEEE Transactions on Antennas and Propagation*, vol. 60, no. 2, pp. 1126–1131, 2011.

[15] K. W. Cho, M. H. Mazaheri, J. Gummeson, O. Abari, and K. Jamieson, "mmwall: A reconfigurable metamaterial surface for mmwave networks," in *HotMobile '21*, pp. 119–125, 2021.

[16] K. W. Cho, Y. Ghasempour, and K. Jamieson, "Towards dual-band reconfigurable metamaterial surfaces for satellite networking," *arXiv preprint arXiv:2206.14939*, 2022.

[17] B. Liu, S. Li, Y. He, Y. Li, and S.-W. Wong, "Generation of an orbital-angular-momentum-mode-reconfigurable beam by a broadband 1-bit electronically reconfigurable transmitarray," *Physical Review Applied*, vol. 15, no. 4, p. 044035, 2021.

[18] K. Guo, Q. Zheng, Z. Yin, and Z. Guo, "Generation of mode-reconfigurable and frequency-adjustable oam beams using dynamic reflective metasurface," *IEEE Access*, vol. 8, pp. 75523–75529, 2020.

[19] J. Han, L. Li, H. Yi, and W. Xue, "Versatile orbital angular momentum vortex beam generator based on reconfigurable reflective metasurface," *Japanese journal of applied physics*, vol. 57, no. 12, p. 120303, 2018.

[20] F. Mao, M. Huang, J. Yang, C. Yang, T. Li, and J. Zhang, "Capacity performance of wireless oam-based massive mimo system," *Progress In Electromagnetics Research M*, vol. 82, pp. 149–156, 2019.

[21] G. Xie, Z. Zhao, Y. Yan, L. Li, Y. Ren, N. Ahmed, Y. Cao, A. J. Willner, C. Bao, Z. Wang, *et al.*, "Demonstration of tunable steering and multiplexing of two 28 ghz data carrying orbital angular momentum beams using antenna array," *Scientific reports*, vol. 6, no. 1, pp. 1–9, 2016.

[22] Z. H. Jiang, L. Kang, W. Hong, and D. H. Werner, "Highly efficient broadband multiplexed millimeter-wave vortices from metasurface-enabled transmit-arrays of subwavelength thickness," *Physical Review Applied*, vol. 9, no. 6, p. 064009, 2018.

[23] Y. Peng, L. Shangguan, Y. Hu, Y. Qian, X. Lin, X. Chen, D. Fang, and K. Jamieson, "Plora: A passive long-range data network from ambient lora transmissions," in *Proceedings of the 2018 Conference of the ACM Special Interest Group on Data Communication*, pp. 147–160, 2018.